Distortions in the Surface of Last Scattering

Peikai Li,[1] Scott Dodelson,[1] and Wayne Hu[2]

[1] *Department of Physics, Carnegie Mellon University, Pittsburgh, Pennsylvania 15312, USA*
[2] *Kavli Institute for Cosmological Physics, Department of Astronomy & Astrophysics, Enrico Fermi Institute, The University of Chicago, Chicago, IL 60637, USA*

(Dated: March 28, 2019)

The surface of last scattering of the photons in the cosmic microwave background is **not** a spherical shell. Apart from its finite width, each photon experiences a different gravitational potential along its journey to us, leading to different travel times in different directions. Since all photons were released at the same cosmic time, the photons with longer travel times started farther away from us than those with shorter times. Thus, the surface of last scattering is corrugated, a deformed spherical shell. We present a quadratic estimator that could provide a map of the time delays as a function of position on the sky. The signal to noise of this map could exceed unity on large scales.

DISTANCE TO THE LAST SCATTERING SURFACE

The theory of general relativity dictates that particles traveling through gravitational potential wells experience time delays [**?**]. If two photons are emitted at the same time, then they will travel different distances depending upon the potential Φ through which they travel. In the cosmological context of an expanding, spatially flat background? , the fractional difference in comoving distance D_* to a source at redshift z_* is

$$d(\hat{n}) = \frac{2}{D_*}\int_0^{D_*} dD\,\Phi\left(D\hat{n}; t(D)\right) \tag{1}$$

where $t(D)$ is the age of the universe when the photon is a comoving distance D from us, and we use the space-time metric convention

$$ds^2 = -(1+2\Phi)dt^2 + a^2(1-2\Phi)d\vec{x}^2 \tag{2}$$

with $a(t)$ the scale factor. Note the sign in Eq. (1): if photons pass through an over-dense region where $\Phi < 0$, then they experience a time delay and therefore they arrive from a closer distance than the unperturbed last scattering surface[1].

Photons that comprise the cosmic microwave background (CMB) experience these same time delays or advances [**?**] where z_* is the redshift corresponding to the last scattering surface. Since photons do not decouple instantaneously from the electron-proton plasma, the surface of last scattering is often said to have a finite width, and a more accurate expression for the fractional difference in distance traveled is

$$d(\hat{n}) = 2\int_0^{\infty} dz\, e^{-\tau(z)}\, K_d(z)\Phi\left(D(z)\hat{n}; t(z)\right) \tag{3}$$

where $H(z)$ is the Hubble expansion rate; $K_d(z) = (H(z)D_*)^{-1}$ and $D_* = \int_0^{\infty} dz' e^{-\tau(z')}/H(z')$. with τ being the optical depth, ignoring reionization, which becomes very large at times smaller than the epoch of last scattering, t_* or equivalently when $z > z_*$.

This directional-dependent change in the distance to last scattering implies that the last scattering surface is not a simple spherical shell. There are two other well-studied phenomena that undercut the notion that the photons in the CMB freely streamed to us from a infinitely thin last scattering sphere. First, since the mean free path at recombination was finite, the last scattering surface has a finite width, and this is accounted for in all computations of CMB anisotropies. Second, the photons in the CMB experience angular deflections as they traverse the inhomogeneous universe [**? ?**] and this effect has been exploited by recent experiments [**? ? ? ? ?**] that make maps of the projected gravitational potential.

Although deflections and delays are two different phenomena, they share some similarities, especially in the case of the CMB. Both are determined by the integrated potential along the line of sight, although with slightly different kernels, as depicted in Figure 1: the integrated potential ϕ that determines deflections has the same form as the right-hand side of Eq. (3) with

$$K_\phi(z) = \frac{D_* - D(z)}{D(z)D_*H(z)}. \tag{4}$$

It is clear that they will be highly correlated, so as a first approximation, we might view the maps of the lensing potential created for example in **?**] as maps of distance to the last scattering surface. Another similarity, one that has not yet been exploited, is that the quadratic estimator formalism [**?**] can be applied to the delays as well, and this is what we will do in this paper. We start though with the rather daunting facts that the RMS fractional distance differences are a factor of ten smaller than the RMS angular deviations and their impact on CMB power spectra is even smaller [**?**]. Further, while the latter peaks at degree scales, the former peak on the largest scales where cosmic variance is higher.

[1] There is also a geometric time delay that is typically of the same size for a single lens but is much smaller here on the large scales of interest.

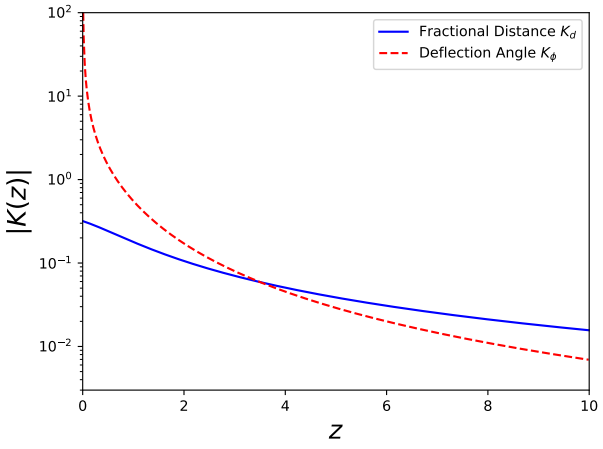

FIG. 1. Kernel that weights the integral of the gravitational potential for the time delay examined here and the more carefully studied deflection angle.

EFFECT OF DISTANCE CHANGES ON THE CMB

The observed temperature in a given direction $\Theta^{\rm obs}(\hat{n})$ is the undistorted temperature $\tilde{\Theta}(\hat{n})$ plus the deflection due to gravitational lensing plus a term proportional to the small fractional difference $d(\hat{n})$

$$\Theta^{\rm obs}(\hat{n}) = \tilde{\Theta}(\hat{n}) - \nabla_i\phi(\hat{n})\nabla^i\tilde{\Theta}(\hat{n}) - \frac{\partial\tilde{\Theta}(\hat{n})}{\partial \ln D_*}\, d(\hat{n}). \quad (5)$$

The third term's derivative can be evaluated by recalling that the undistorted temperature can be expanded in spherical harmonics with coefficients

$$\tilde{\Theta}_{lm} = 4\pi(-i)^l \int \frac{d^3k}{(2\pi)^3} Y^*_{lm}(\hat{k}) S(\vec{k};\eta_*) j_l(kD_*), \quad (6)$$

where S is the source function, dominated on small scales by the monopole and dipole, as in Eq. (22) of Ref. [**?**]. The derivative with respect to distance then acts on the spherical Bessel function, and after expanding the fractional difference in spherical harmonics as well, we obtain

$$\Theta^{\rm obs}_{lm} = \tilde{\Theta}_{lm} - \delta\Theta^{\rm defl}_{lm} - \delta\Theta^{\rm dist}_{lm} \quad (7)$$

with the two first order terms due to deflection and the change in distance equal to

$$\delta\Theta^{\rm defl}_{lm} = \sum_{LM}\sum_{l'm'} {}_0I^{mMm'}_{lLl'}\tilde{\Theta}_{l'm'}\phi_{LM}, \quad (8)$$

$$\delta\Theta^{\rm dist}_{lm} = \sum_{LM}\sum_{l'm'} {}_0J^{mMm'}_{lLl'}\frac{\partial\tilde{\Theta}_{l'm'}(D_*)}{\partial \ln D_*} d_{LM}. \quad (9)$$

Here, we have written the integral over the product of three spherical harmonics as ${}_0I$ and ${}_0J$ to enable generalization to the case of polarization, which involves spin $s = 2$ harmonics. The general expression is

$${}_sI^{mMm'}_{lLl'} = (-1)^m \begin{pmatrix} l & L & l' \\ -m & M & m' \end{pmatrix} {}_sF_{lLl'}, \quad (10)$$

$${}_sJ^{mMm'}_{lLl'} = (-1)^m \begin{pmatrix} l & L & l' \\ -m & M & m' \end{pmatrix} {}_sG_{lLl'}, \quad (11)$$

with

$$\begin{aligned} {}_sF_{lLl'} &\equiv \big[L(L+1) - l'(l'+1) + l(l+1)\big] \\ &\quad \times \frac{\big[(2l+1)(2L+1)(2l'+1)\big]^{1/2}}{\sqrt{16\pi}} \begin{pmatrix} l & L & l' \\ s & 0 & -s \end{pmatrix}, \\ {}_sG_{lLl'} &\equiv \frac{\big[(2l+1)(2L+1)(2l'+1)\big]^{1/2}}{\sqrt{4\pi}} \begin{pmatrix} l & L & l' \\ s & 0 & -s \end{pmatrix}. \end{aligned} \quad (12)$$

Note the extra two powers of the multipoles in the function F that governs deflection; these follow from the fact that both the temperature and the potential are differentiated with respect to transverse position on the sky. By contrast, the radial derivative that governs the impact of the time delay, or change in distance to the last scattering surface, appears in Eq. (9) as the logarithmic derivative of the unlensed coefficients $\tilde{\Theta}_{LM}$.

As in the case of the effect of deflections on the CMB, the varying distances to the last scattering surface leads to correlations between l-modes that differ from one another. We proceed as in Ref. [**?**] by focusing on the expectation of off-diagonal $(l_1, m_1 \neq l_2, m_2)$ terms quadratic in the observed moments:

$$\begin{aligned} \langle \Theta^{\rm obs}_{l_1m_1}\Theta^{\rm obs}_{l_2m_2}\rangle &= \sum_{LM}(-1)^M \begin{pmatrix} l_1 & l_2 & L \\ m_1 & m_2 & -M \end{pmatrix} \\ &\quad \times \big[\phi_{LM} f_{l_1Ll_2} + d_{LM} g_{l_1Ll_2}\big], \end{aligned} \quad (13)$$

where

$$\begin{aligned} f_{l_1Ll_2} &\equiv \big[\tilde{C}^{\Theta\Theta}_{l_1}{}_0F_{l_2Ll_1} + \tilde{C}^{\Theta\Theta}_{l_2}{}_0F_{l_1Ll_2}\big], \\ g_{l_1Ll_2} &\equiv \big[\tilde{C}^{\Theta\Theta,d}_{l_1}{}_0G_{l_2Ll_1} + \tilde{C}^{\Theta\Theta,d}_{l_2}{}_0G_{l_1Ll_2}\big]. \end{aligned} \quad (14)$$

The change in distance to the last scattering spectrum produces the spectrum

$$C^{\Theta\Theta,d}_l \equiv \frac{2}{\pi}\int_0^\infty \frac{dk}{k}\,(S(k;\eta_*))^2\, j_l(kD_*)\,\frac{\partial j_l(kD_*)}{\partial \ln D_*} \quad (15)$$

This expression is identical to the one for the undistorted CMB spectrum C_l other than the replacement $j_l \to j'_l$. The two spectra are shown in Fig. 2. We modify the public CAMB code and account for the finite thickness of the last scattering surface, the actual integrand look like:

$$\begin{aligned} &(S(k;\eta_*))^2\, j_l(kD_*)\,\frac{\partial j_l(kD_*)}{\partial \ln D_*} \\ &\to \mathcal{P}_{\rm R}(k) T_\Theta[j_l;k] T^{(1)}_\Theta[j_l;k] \end{aligned} \quad (16)$$

with $\mathcal{P}_{\rm R}$ primitive power spectrum, and $T_\Theta[j_l;k]$ is the transfer function for temperature defined as:

$$T_\Theta[j_l;k] = \int d\eta \mathcal{S}_\Theta(k;\eta) j_l(kD(\eta)). \tag{17}$$

which is the general form of the source function above. $\mathcal{S}_\Theta$ is the modified source function defined in CAMB, we can determine its expression using Eq. (22) of Ref. [**?**] (ignore third term, which is the ISW effect),

$$\begin{aligned} S(\vec{k};\eta_*) j_l(kD_*) &= [\Theta+\Psi](\eta_*) j_l(kD_*) + v_b(k,\eta_*) j_l'(kD_*) \\ \rightarrow T_\Theta[j_l;k] &= \int d\eta \left\{ g(\eta)[\Theta+\Psi](\eta) \right. \\ &\quad \left. -(g(\eta) v_b(k,\eta))' \right\} j_l(kD(\eta)) \end{aligned} \tag{18}$$

with $g(\eta)$ the visibility function, sharply peaked at $\eta = \eta_*$. Approximate $g(\eta)$ as $\delta(\eta-\eta_*)$ we can go back from $T_\Theta[j_l;k]$ to $S(\vec{k};\eta_*)j_l(kD_*)$. And second term comes from integration by parts. Also define $T^{(1)}_\Theta[j_l;k]$ as $j_l(kD)$ in the integrand replaced by $\partial j_l(kD)/\partial \ln D$.

In order to compute $C_l^{\Theta\Theta,d}$ we simply replace $j_l(kD)$ by $\partial j_l(kD)/\partial \ln D$ when calculating the transfer functions and we can get the result.

Note the difference between these two functions. Each involves a derivative. The one that governs deflections, f, involves a derivative with respect to the transverse directions so F as defined in Eq. (12) has more powers of l than does G. The function that governs changes in distances involved a radial derivative, and this shows up in the spectrum $C_l^{\Theta\Theta,d}$.

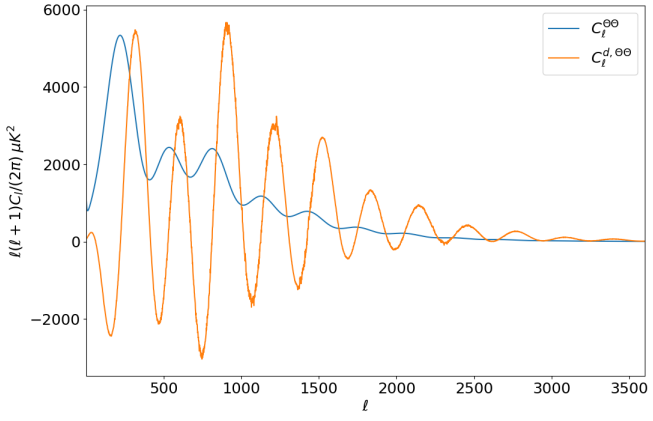

FIG. 2. Spectra of CMB temperature anisotropies and the logarithmic derivative of that spectrum with respect to the distance to the last scattering surface as defined in Eq. (18).

The correlation between different l-modes enables us, following Ref. [**?**], to extract information about the fields causing these correlations by forming quadratic estimators for both the gravitational potential responsible for deflections and the fractional distance field:

$$\begin{aligned} \hat{\phi}_{LM} &= A_L \sum_{l_1 m_1} \sum_{l_2 m_2} \\ &\quad (-1)^M \begin{pmatrix} l_1 & l_2 & L \\ m_1 & m_2 & -M \end{pmatrix} h^\phi_{l_1 l_2}(L) \Theta^{\rm obs}_{l_1 m_1} \Theta^{\rm obs}_{l_2 m_2} \end{aligned} \tag{19}$$

$$\begin{aligned} \hat{d}_{LM} &= B_L \sum_{l_1 m_1} \sum_{l_2 m_2} \\ &\quad (-1)^M \begin{pmatrix} l_1 & l_2 & L \\ m_1 & m_2 & -M \end{pmatrix} h^d_{l_1 l_2}(L) \Theta^{\rm obs}_{l_1 m_1} \Theta^{\rm obs}_{l_2 m_2} \end{aligned} \tag{20}$$

where

$$h^\phi_{l_1 l_2}(L) \equiv \frac{f_{l_1 L l_2}}{2 C_{l_1} C_{l_2}} \tag{21}$$

$$h^d_{l_1 l_2}(L) \equiv \frac{g_{l_1 L l_2}}{2 C_{l_1} C_{l_2}} \tag{22}$$

and

$$A_L \equiv (2L+1) \left\{ \sum_{l_1 l_2} h^\phi_{l_1 l_2}(L) f_{l_1 L l_2} \right\}^{-1} \tag{23}$$

$$B_L \equiv (2L+1) \left\{ \sum_{l_1 l_2} h^d_{l_1 l_2}(L) g_{l_1 L l_2} \right\}^{-1}. \tag{24}$$

With these definitions, the expectation values of the two estimators are equal to ϕ_{LM} and d_{LM} respectively.

The noise on these estimators is now given by the prefactors A_L and B_L, so

$$\langle \hat{d}_{LM} \hat{d}^*_{L'M'} \rangle = \delta_{LL'} \delta_{MM'} \left(C_L^{dd} + B_L \right) \tag{25}$$

with the first term on the right the signal and the second the noise. Fig. 3 shows the signal and noise at each L for several experimental configurations.

An estimate of the detectability of this signal can be obtained by computing the projected error, σ_d, on the amplitude A^d of the power spectrum $A^d C_L^{dd}$, where the fiducial model has $A^d = 1$. This is given by summing over all multipoles:

$$\left(\frac{1}{\sigma_d} \right)^2 = \sum_L^\infty \frac{(2L+1) f_{\rm sky}}{2} \left(\frac{C_L^{dd}}{C_L^{dd} + B_L} \right)^2. \tag{26}$$

Fig. 3 shows that most of the signal comes from the lowest L-modes, particularly $L = 1$. However, even for a full-sky experiment and the most optimistic noise projections, the signal will not be detectable using temperature only. Wayne: please check if this rewording is what you had in mind. Peikai: if we agree on this notation, please relabel the y-axis on figure 4 as "Time Delay Detectability (σ_d)"

POLARIZATION

The estimator above used only the temperature anisotropy field, but the polarization field contains even more information about the lensing potential that governs deflection and distance changes. This was worked

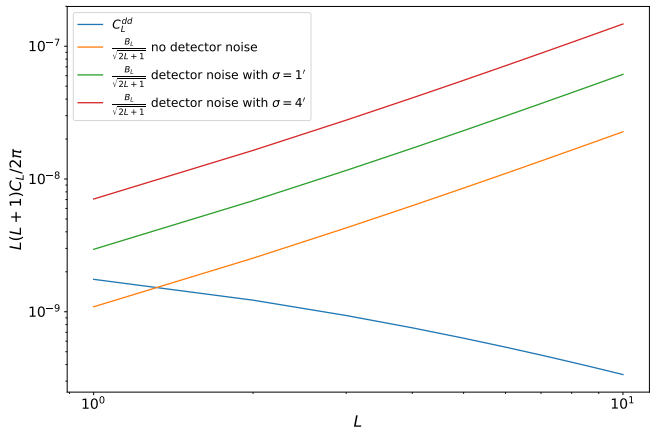

FIG. 3. Signal (decreasing blue curve) due to the distorted surface of last scattering and the noise using the quadratic estimator constructed from the small scale temperature anisotropy ($\Theta\Theta$ in the notation of Table 1) for several different experimental configurations. Most optimistic is no noise out to $l_{\rm max} = 7000$; the other two noise curves have sensitivity of 1μK-arcmin and beam size. $\theta_{\rm FWHM} = 1'$ or $4'$. Here, $f_{\rm sky}$ is set to one.

out in detail by Ref. [**?**] for deflection, and we follow their notation here. There are now three fields of interest: temperature Θ, and the two fields associated with polarization, E and B. With letters a, b each ranging over these three fields, we have

$$\langle a^{obs}_{l_1 m_1} b^{obs}_{l_2 m_2}\rangle = \sum_{LM} (-1)^M \begin{pmatrix} l_1 & l_2 & L \\ m_1 & m_2 & -M \end{pmatrix} \times \left[\phi_{LM} f^\alpha_{l_1 L l_2} + d_{LM} g^\alpha_{l_1 L l_2}\right]. \quad (27)$$

The functions f^α and g^α are the generalizations of Eq. (14) to include polarization (Eq. (14) now corresponds to $\alpha = \Theta\Theta$). The full set of f^α was determined by Ref. [**?**] and is reproduced in Table 1, which now includes the full set of g^α that govern the impact of changing radial distances. Note that $\tilde{C}_l$ corresponds to the spectra of the unlensed fields; and $\tilde{C}_l^{\Theta\Theta,d}$ for example is the radial derivative of the unlensed spectrum.Note that the angular deflection coefficients f^α do not carry superscript ^{d} because the derivatives are transverse and therefore captured by powers of ℓ. The radial derivatives in the g^α must be computed directly, as in Eq. (18) and Eq. (29). For example,

$$C_l^{\Theta E,d} \equiv \frac{2}{\pi}\int_0^\infty \frac{dk}{k}\,\mathcal{P}_R(k)\left\{T_\Theta[j_l;k]T_E^{(1)}[j_l^{(22)};k] + T_\Theta^{(1)}[j_l;k]T_E[j_l^{(22)};k]\right\}/2 \quad (28)$$

similarly with

$$T_E[j_l^{(22)};k] = \int d\eta \mathcal{S}_E(k;\eta) j_l^{(22)}(kD(\eta))$$
$$T_E^{(1)}[j_l^{(22)};k] = \int d\eta \mathcal{S}_E(k;\eta)\frac{\partial j_l^{(22)}(kD(\eta))}{\partial \ln D(\eta)}. \quad (29)$$

$\mathcal{S}_E$ is the modified E-mode source function and radial function $j_l^{(22)}(x) \propto j_l(x)/x^2$, notice we only include scalar mode here. See Ref. [**?**] for a more detailed discussion.

α	$f^\alpha_{l_1 L l_2}$	$g^\alpha_{l_1 L l_2}$
$\Theta\Theta$	$\tilde{C}^{\Theta\Theta}_{l_1}{}_0F_{l_2 L l_1} + \tilde{C}^{\Theta\Theta}_{l_2}{}_0F_{l_1 L l_2}$	$\tilde{C}^{\Theta\Theta,d}_{l_1}{}_0G_{l_2 L l_1} + \tilde{C}^{\Theta\Theta,d}_{l_2}{}_0G_{l_1 L l_2}$
ΘE	$\tilde{C}^{\Theta E}_{l_1}{}_2F_{l_2 L l_1} + \tilde{C}^{\Theta E}_{l_2}{}_0F_{l_1 L l_2}$	$\tilde{C}^{\Theta E,d}_{l_1}{}_2G_{l_2 L l_1} + \tilde{C}^{\Theta E,d}_{l_2}{}_0G_{l_1 L l_2}$
EE	$\tilde{C}^{EE}_{l_1}{}_2F_{l_2 L l_1} + \tilde{C}^{EE}_{l_2}{}_2F_{l_1 L l_2}$	$\tilde{C}^{EE,d}_{l_1}{}_2G_{l_2 L l_1} + \tilde{C}^{EE,d}_{l_2}{}_2G_{l_1 L l_2}$
ΘB	$i\tilde{C}^{\Theta E}_{l_1}{}_2F_{l_2 L l_1}$	$i\tilde{C}^{\Theta E,d}_{l_1}{}_2G_{l_2 L l_1}$
EB	$i[\tilde{C}^{EE}_{l_1}{}_2F_{l_2 L l_1} - \tilde{C}^{BB}_{l_2}{}_2F_{l_1 L l_2}]$	$i[\tilde{C}^{EE,d}_{l_1}{}_2G_{l_2 L l_1} - \tilde{C}^{BB,d}_{l_2}{}_2G_{l_1 L l_2}]$
BB	$\tilde{C}^{BB}_{l_1}{}_2F_{l_2 L l_1} + \tilde{C}^{BB}_{l_2}{}_2F_{l_1 L l_2}$	$\tilde{C}^{BB,d}_{l_1}{}_2G_{l_2 L l_1} + \tilde{C}^{BB,d}_{l_2}{}_2G_{l_1 L l_2}$

TABLE I. Explicit forms for f anb h of various polarizations. Notice that for TT, TE, EE and BB polarization these functions are "even"; for TB and EB polarization they are "odd" instead. "Even" and "Odd" indicate that the functions are non-zero only when $l_1 + l_2 + L$ are even or odd, respectively.

An estimator can now be constructed for each of the pairs of fields (except BB), so letting α denote pairs of fields (ab), we have

$$\hat{d}^\alpha_{LM} = (-1)^M B^\alpha_L \sum_{l_1 m_1}\sum_{l_2 m_2}\begin{pmatrix} l_1 & l_2 & L \\ m_1 & m_2 & -M \end{pmatrix} \times h^{\alpha,d}_{l_1 l_2}(L) a^{obs}_{l_1 m_1} b^{obs}_{l_2 m_2}, \quad (30)$$

where the coefficients are generalizations of Eq. (24) with g and h there acquiring superscripts α. The g^α are given in Table 1 and the minimizing weights are

$$h^{\alpha=(ab),d}_{l_1 l_2}(L) = \frac{C^{aa}_{l_2} C^{bb}_{l_1} g^{\alpha *}_{l_1 L l_2} - (-1)^{L+l_1+l_2} C^{ab}_{l_1} C^{ab}_{l_2} g^{\alpha *}_{l_2 L l_1}}{C^{aa}_{l_1} C^{aa}_{l_2} C^{bb}_{l_1} C^{bb}_{l_2} - (C^{ab}_{l_1} C^{ab}_{l_2})^2} \quad (31)$$

with

$$h^{\alpha=(aa),d}_{l_1 l_2}(L) = \frac{g^{\alpha *}_{l_1 L l_2}}{2 C^{aa}_{l_1} C^{aa}_{l_2}}. \quad (32)$$

Note that in the special case when $C^{ab}_l = 0$ (e.g., for ΘB or EB), this reduces to

$$h^{\alpha,d}_{l_1 l_2}(L) \to \frac{g^{\alpha *}_{l_1 L l_2}}{C^{aa}_{l_1} C^{bb}_{l_2}}. \quad (33)$$

The covariance of these quadratic estimators

$$\langle \hat{d}^{\alpha *}_{LM} d^\beta_{L'M'}\rangle \equiv \delta_{LL'}\delta_{MM'}\left[C^{dd}_L + N^{d,\alpha\beta}_L\right] \quad (34)$$

with Gaussian noise given by

$$N^{d,\alpha\beta}_L = \frac{B^{\alpha *}_L B^\beta_L}{2L+1}\sum_{l_1 l_2}\left\{h^{\alpha,d*}_{l_1 l_2}(L)\left[C^{ac}_{l_1} C^{bd}_{l_2} h^{\alpha,d}_{l_1 l_2}(L) + (-1)^{L+l_1+l_2} C^{ad}_{l_1} C^{bc}_{l_2} h^{\beta,d}_{l_2 l_1}(L)\right]\right\} \quad (35)$$

with $\alpha = (ab)$, $\beta = (cd)$. For $\alpha = \beta$, Eq. (40) reduces to $N_L^{d,\alpha\alpha} = B_L^\alpha$. Armed with these expressions, we can form a minimum variance estimator

$$\hat{d}^{\rm mv}_{LM} = \sum_\alpha \omega^\alpha(L)\hat{d}^\alpha_{LM} \tag{36}$$

with weights and variance given by

$$\omega^\alpha(L) = N_L^{d,\rm mv}\sum_\beta (N_L^{d,-1})^{\alpha\beta} \tag{37}$$

$$N_L^{d,\rm mv} = \frac{1}{\sum_{\alpha\beta}(N_L^{d,-1})^{\alpha\beta}} \tag{38}$$

where $N_L^{d,-1}$ is the inverse matrix of time delay noise given by Eq. (27), with matrix indices given by polarizations.

We saw in Fig. 3 that small scale temperature maps only are not sufficient to detect this signal convincingly. To assess the added information contained in the polarization field, we show the detectability in the form of σ_d for the lowest L-modes ($L \leqslant 5$, which contributes all of the signal) as a function $l_{\rm max}$ for a noiseless experiment in Fig. 4.

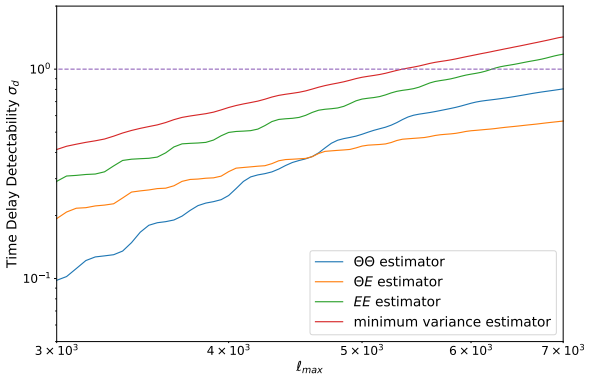

FIG. 4. Detectability of the spectrum of the time delay signal, σ_d, using Eq. (26) for different quadratic estimators as a function of the largest l-mode accessed. Here we set $f_{\rm sky}$ to be 1.

Here we keep $l_{\rm min}$ fixed at 1000 for the CMB fields (we tested that our final results are insensitive to this choice) and let $l_{\rm max}$ vary. We can see that at $l_{\rm max} \approx 5000$, the minimum variance estimator detectability reaches 1, but of course this is for the most optimistic of configurations. Any comments on the differences between lensing and delay estimators especially on B modes? According to Appendix B of Ref. [**?**], we can see that wigner-3j with odd l_1+l_2+L is much smaller than its even counterpart. Unlike the deflection case, we don't have a compensation term in front. This would result in a much smaller detectability for estimators with B-modes, so we don't include those in Fig. 4.

CROSS POWER SPECTRUM

The auto-spectrum of the distortion field, d, will apparently be very challenging to extract. Another possibility is to cross-correlate the quadratic estimator for the distortion field with other fields that are well-measured. Cross-correlations can be more easily detected if the two-fields are highly correlated and one of the fields can be detected with high signal to noise.

As a first attempt, we consider the cross-spectrum of the distance distortion field with the projected potential responsible for deflections, ϕ. An estimator for this cross-spectrum is

$$\hat{C}^{\phi d,\alpha\beta}_{LM} = \hat{\phi}^{\alpha*}_{LM}\hat{d}^\beta_{LM} - N_L^{c,\alpha\beta}, \tag{39}$$

c stands for cross here; where the bias is equal to the noise is

$$N_L^{c,\alpha\beta} = \frac{A_L^{\alpha*}B_L^\beta}{(2L+1)}\sum_{l_1l_2}\Big\{h^{\alpha,\phi*}_{l_1l_2}(L)\big[C^{ac}_{l_1}C^{bd}_{l_2}h^{\alpha,d}_{l_1l_2}(L) + (-1)^{L+l_1+l_2}C^{ad}_{l_1}C^{bc}_{l_2}h^{\beta,d}_{l_2l_1}(L)\big]\Big\} \tag{40}$$

Gaussian covariance of $\hat{C}^{\phi d,\alpha\beta}_{LM}$ is

$$\begin{aligned}
&\langle \hat{C}^{\phi d,\alpha\beta*}_{LM}\hat{C}^{\phi d,\gamma\sigma}_{LM} - (C_L^{\phi d})^2\rangle/(2L+1)\\
&= \Big\{(C_L^{\phi d}+N_L^{c,\alpha\beta})(C_L^{\phi d}+N_L^{c,\gamma\sigma})\\
&\quad +(C_L^{\phi d}+N_L^{c,\alpha\sigma})(C_L^{\phi d}+N_L^{c,\beta\gamma})\\
&\quad +(C_L^{\phi\phi}+N_L^{\phi,\alpha\gamma})(C_L^{dd}+N_L^{d,\beta\sigma})\\
&\quad -(C_L^{\phi d}+N_L^{c,\alpha\beta})N_L^{c,\gamma\sigma} - (C_L^{\phi d}+N_L^{c,\gamma\sigma})N_L^{c,\alpha\beta}\\
&\quad +N_L^{c,\alpha\beta}N_L^{c,\gamma\sigma} - (C_L^{\phi d})^2\Big\}/(2L+1)
\end{aligned} \tag{41}$$

When $(\alpha\beta) = (\gamma\sigma)$, this simplifies to

$$\frac{1}{2L+1}\Big\{(C_L^{\phi d}+N_L^{c,\alpha\beta})^2 + (C_L^{\phi\phi}+N_L^{\phi,\alpha\alpha})(C_L^{dd}+N_L^{d,\beta\beta})\Big\} \tag{42}$$

Given these expressions, the best detectability of the cross power spectrum we can reach, defined again as the fractional error on amplitude of this spectrum, is

$$(\sigma_{\rm cross})^{-2} = \sum_L (2L+1)f_{\rm sky} \times \frac{(C_L^{\phi d})^2}{(C_L^{\phi d}+N_L^{c,\rm mv})^2 + (C_L^{\phi\phi}+N_L^{\phi,\rm mv})(C_L^{dd}+N_L^{d,\rm mv})}. \tag{43}$$

We set $f_{\rm sky} = 1$ and sum up tp $L = 100$ to find the detectability, as shown in Fig. 5. We could see that in this ideal case, S/N could reach about 2.5, which still may not be detectable.

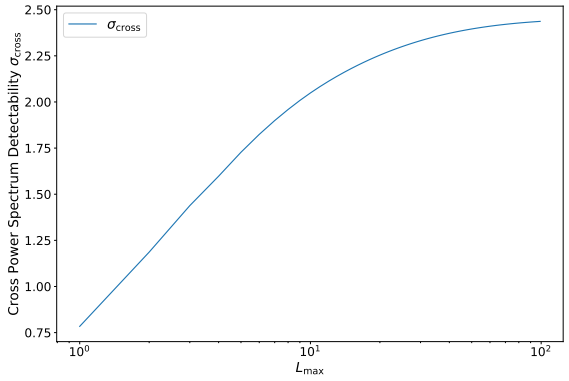

FIG. 5. The detectability of the cross power spectrum of the distance distortion field and the potential inducing deflections as a function of $L_{\rm max}$. Unlike the auto-spectrum, there is signal out to $L_{\rm max} \sim 100$, but the contributions to the detectability plateau after that, so the best that can be hoped for with this cross spectrum is a 3-sigma detection. We still set $l_{\rm max} = 7000$ for all three noise terms.

CONCLUSIONS

The last scattering surface of the CMB is not purely spherical due to the different travel times experienced by photons as they traverse the inhomogeneous gravitational potential. In principle, these distortions in the distance to different directions is detectable, but we conclude here that the standard auto-correlation techniques will not be sufficient to enable detection in the near future. There is the possibility of cross-correlating a map of the distance distortions constructed with the quadratic estimators introduced here with another map of a closely related integrated potential and extracting the signal in that way. Indeed, this was the way that the transverse distortions in the CMB were first detected [**?**]. Here, we have considered the cross-correlation signal between the distance distortion and the standard transverse deviation maps cand concluded that even an all-sky experiment with superior angular resolution would be detect the cross-spectrum at only 3-sigma. We leave exploration of other cross-correlations for further work; however, we point out that yet another challenge confronted will be the fidelity of the distance distortion maps, as they are contaminated by the standard lensing signals.